A comparative analysis of helicopter recovery maneuvers on a SFS by means of PIV and balance measurements

J.C. Matías[1*†], R. Bardera[2*], S. Franchini[3†], E. Barroso[4*], S. Sor[5*]
Instituto Nacional de Técnica Aeroespacial (INTA), Torrejón de Ardoz, Madrid, Spain
†Universidad Politécnica de Madrid (UPM), ETSIAE, Madrid, Spain

A B S T R A C T

The flow field around a frigate is complex due to flow detachments, high velocity gradients, and flow unsteadiness. These flow patterns can endanger helicopter operations around frigates and increase pilot workload above the flight deck. This paper contains a comparative analysis of three different recovery maneuvers: an approach from the stern in the centerline plane (S); a diagonal maneuver (D); and an L-shaped maneuver. The comparison is made using wind tunnel tests with a scaled frigate and a motorized helicopter. For the three maneuvers, velocity contours around the helicopter with Particle Image Velocimetry are obtained. An internal balance is also used to obtain forces and moments on the helicopter during the flight path of the maneuvers. From that measurements, it is concluded that the wake of the ship mostly affects longitudinal and thrust forces. In addition, pitch torque is highly reduced when the helicopter is behind the frigate superstructure, and the roll moment is also important when the wind angle of incidence increases. In the end, an estimation of pilot workload is presented to conclude that L-shaped maneuver is the best for 0º and positive WOD angles and D or S recoveries for negative WOD angles.

Keywords:
PIV, Forces, Frigate, Helicopter recovery

[1] Aerospace engineer, Experimental Aerodynamics, matiasgjc@inta.es
[2] PhD Aerospace Engineering, Experimental Aerodynamics, barderar@inta.es
[3] PhD Aerospace Engineering, Politechnical University of Madrid, s.franchini@upm.es
[4] Aerospace engineer, Experimental Aerodynamics, barrosobe@inta.es
[5] PhD Aerospace Engineering, Experimental Aerodynamics, sors@inta.es

Nomenclature

U_∞	=	Free-stream velocity (m/s)
C_i	=	Forces Coefficient ($i = x, y, z$)
$\lvert C_i \rvert$	=	Force modulus ($i = x, y, z$)
C_{mi}	=	Torque coefficient ($i = x, y, z$)
C_x	=	Longitudinal force coefficient
C_y	=	Lateral force coefficient
C_z	=	Thrust coefficient
C_{mx}	=	Roll coefficient
C_{my}	=	Pitch coefficient
C_{mz}	=	Yaw coefficient
D	=	Rotor Diameter (m)
F_i	=	Force component $i = (x, y, z)$
M_i	=	Torque component $i = (x, y, z)$
g	=	Gravity constant (9.81 m/s^2)
C_T	=	Rotor thrust coefficient
M	=	Helicopter weight (kg)
R	=	Rotor radius (m)
R_s	=	Scaled rotor radius (m)
S	=	Rotor surface (m^2)
T_{io}	=	Rotor thrust (N)
V^*	=	Non-dimensional velocity
V_{tunel}	=	Velocity in the wind tunnel test section
ρ	=	air density (kg/m^3)
Ω	=	Real rotor rotating speed
Ω_s	=	Scaled rotor rotating speed
σ_{C_i}	=	Standard deviations of the components $i = (x, y, z)$

CFD = Computational Fluid Dynamics

FFT = Fast Fourier Transform

PW = Pilot workload parameter

$SFS2$ = Simple Frigate Shape 2

WOD = Wind Over the Deck (º)

1. Introduction

The most significant capability of helicopters is their ability to hover close to objects and structures. And hovering flight is commonly used for rescue missions, as well as military operations. The non-stationary aerodynamic environment generated around structures such as buildings [1], oil rigs [2], military frigates [3], or aircraft carriers [4] can make these operations complex for the pilots. This is because non-aerodynamic structures generate flow detachments, high velocity gradients and turbulence intensities that have a direct effect in the helicopter stability. The specific case of aerodynamic flow around frigates is a widely analyzed topic [5-12]. Different studies about the structure of the frigate air wake [5, 6], numerical and experimental simulations of the wake unsteadiness [7-9], velocity data [10, 11], and turbulent flow measurements on the wake [12] can be founded.

Operating inside the unsteady flows generated by a frigate, the helicopter pilot must make corrections for controlling the aircraft during the recovery maneuver, increasing its workload. Lee and Zan [13, 14] demonstrated that low frequency oscillations (0.2 to 2 Hz) are the ones that most affect the proper helicopter operation. Evaluate the flow frequencies and those induced in the helicopter operation can be performed in different ways. By numerical analysis using Computational Fluid Dynamics, to develop a model of the helicopter-ship dynamic interference [15], or a model of a hovering main rotor operating near ship structures [16]. Another possibility to carry out experimental tests in wind tunnel with scaled models, taking velocity measurements with PIV (Particle Image Velocimetry) to investigate the ship airwake and rotor downwash flowfield [17, 18].

Another type of wind tunnel testing involves the use of balances to measure aerodynamic forces and moments [19-23]. For example, the interference between CH-46 tandem helicopter and V-22 tilt-rotors in a shipboard environment is analyzed in [19, 20]. Wang et al. performed a similar approach to evaluate the aerodynamic effect of a ship superstructure during helicopter operations [21, 22]. They described the design, calibration, and application of AirDyn, a six-component dynamic force balance mounted in a 1/54th scale helicopter, created for water tunnel force measurements. Finally, a recent study [23] investigate numerically and experimentally the behavior of unsteady aerodynamic loads on a scaled helicopter when is operating inside the air wake of a generic frigate model. The data extracted from the above mentioned studies can be included in high-fidelity helicopter simulators [24-28] in order to evaluate the pilot risk and the increase in workload during the procedures, and make them safer in the future.

This paper aims to present wind tunnel measurements to improve the understanding of the helicopter and frigate aerodynamic interaction, comparing three ways of helicopter recovery maneuvers on a frigate. For that, 1/100 Scaled models of frigate and a motorized helicopter is tested extracting PIV images of the flow and forces and moments using HELIBAL, an internal six-component balance specifically designed, manufactured and calibrated at INTA. The PIV velocity contours and the force measurements will allow comparison of three different helicopter recovery maneuvers over the frigate (stern, diagonal and L-shaped), and the possible pilot workload during these maneuvers. The effect of the wind angle of incidence has been also analyzed, simulating wind conditions between 0 and 30º, with both winds from the port and starboard side.

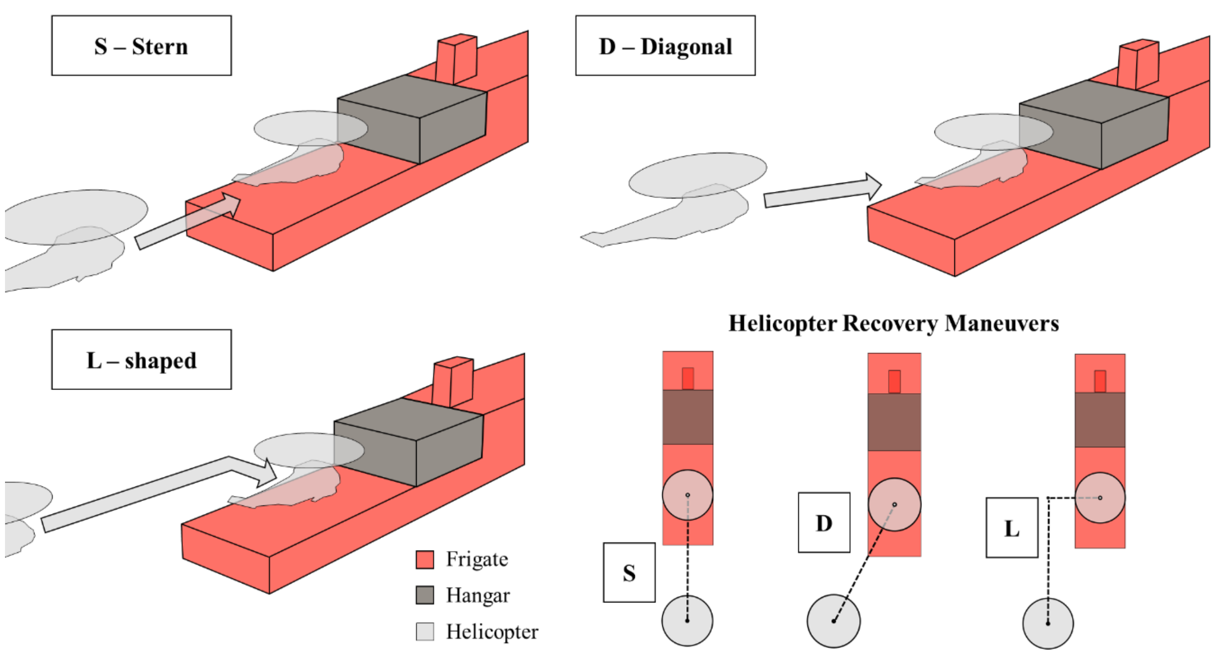

Fig. 1 Helicopter recovery path during stern (S), diagonal (D) and L-shaped (L) maneuvers.

2. Helicopter recovery maneuvers

Military helicopter pilots can perform different recovery maneuvers on a frigate [29]. Three common approaches are displayed in figure 1, which are the ones analyzed in detail in this comparative analysis of maneuvers. The simplest way is the stern approach (S), in which the helicopter lands directly from the stern through the centerline plane of the frigate. The second option is to perform a diagonal maneuver (D) from the port side of the frigate. And finally, a third option is to approach in a L-shaped path (L) from the port side. All maneuvers have in common an approach until a hovering position, and a final descend to deck at the landing spot.

3. Experimental Set-up

3.1. Wind Tunnel INTA-T1 and Particle Image Velocimetry (PIV)

At the National Institute for Aerospace Technology (INTA), there is the low-speed wind tunnel T1, figure 2. It has a closed circuit and elliptical open test section of 2 m × 3 m. Using a maximum power of 420 kW, the air inside the wind tunnel test section can reach up to 60 m/s with turbulence intensity under 0.5 %.

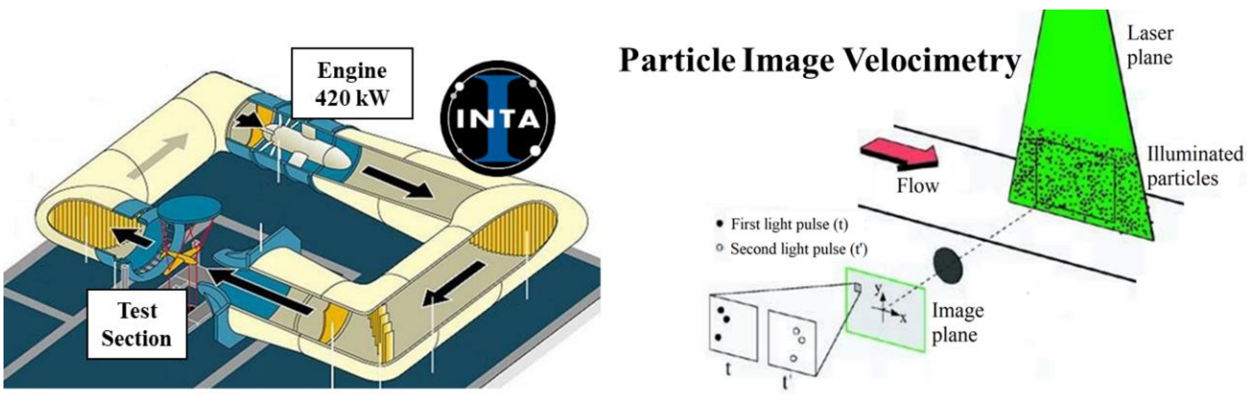

Fig. 2 Wind Tunnel T1 (INTA) and Particle Image Velocimetry (PIV) working scheme

Flow visualization tests when the scaled helicopter is operating above the frigate are obtained with a Particle Image Velocimetry system, or PIV [30-34], installed in the wind tunnel test section. It is a velocity measurement technique based on illuminating small tracer particles of ∼1 μm in diameter seeded in the flow with two Nd: YAG pulsed lasers. The working scheme of the system is displayed in figure 2. A digital camera composed by a 2048 × 2048 pixels CCD sensor, synchronized with the laser pulses, captures pairs of images that records the positions of the particles. The first capture (t) and second capture (t') of the image pair can be correlated using Fast Fourier Transform (FFT) inside small interest windows selected of 32 × 32 pixels in size, to obtain the average displacement of the particles in each one. The magnification factor was $M = 1876$ pix $/470$ mm, and the field of view 512 mm. From this correlation, an averaged displacement vector for each window is known and as the time between captures is also adjusted ($\Delta t = 25$ μs), the velocity can be determined. All the velocity contours were obtained from a total of 100 pairs of images averaged and represented in non-dimensional velocity contours using Tecplot360 software.

3.2. Simple Frigate Shape 2 and helicopter

To generalize the results obtained in this comparative analysis, a standard frigate model is used, specifically a Simple Frigate Shape 2 (SFS2) at 1:100th scaled size, figure 3.

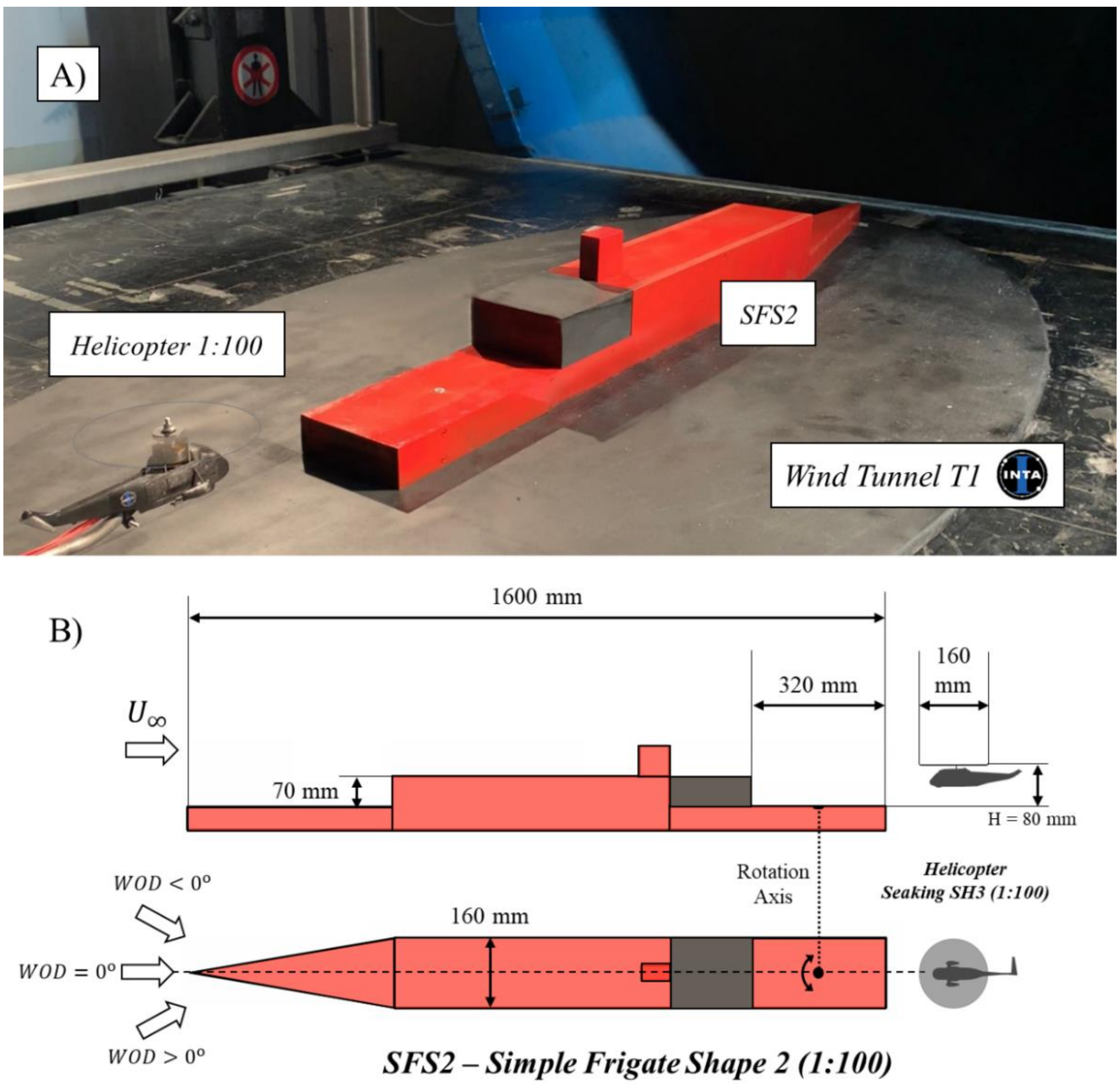

Fig. 3 A) SFS2 and helicopter model at the wind tunnel test section B) Models dimensions.

The SFS was proposed by a ship air wake modeling working group within the Technical co-operation Program (TTCP) with the goal of performing advances in frigate aerodynamic research [35-38]. It represents the above waterline parts of the hull, the bow, the superstructure, and the helicopter flight deck at the stern. The location of this flight deck, just behind the non-aerodynamic superstructure, is the cause of the presence of areas of low velocities, detached flows, and high velocity gradients on the deck that can affect the safety of helicopter recovery maneuvers. The dimensions of the model used for testing are displayed in figure 3 B, with a total length of 1600 mm, a beam of 160 mm, and 320 mm of the flight deck length. The helicopter model is based on a 1:100 Sikorski Sea King SH-3, commonly used for operations above frigates. Its scaled rotor diameter has 160 mm, and the simulated height of the rotor during the recovery maneuvers is constant ($H = 80$ mm). A photograph taken during the tests and inside the wind tunnel test section is also shown in figure 3 A.

In order to simulate different cases of wind over the deck (WOD), the full experimental set-up (frigate and helicopter) can be rotated around an axis located in the center of the flight deck (figure 3 B). Thus, tests are carried out at WOD angles of -30º, -20º, -10º, 0º, 10º, 20º, and 30º, being positive if the wind comes from the port side and negative when it comes from the starboard side. Regardless the angle, the helicopter is always aligned with the centerline plane of the frigate.

3.3. HELIBAL

HELIBAL (HELIcopter BALance) is a six-components internal balance designed specifically for integrating inside a 1:100 scaled helicopter measuring 3 forces (thrust, lateral, and drag) and 3 moments (pitch, yaw, and roll) during wind tunnel tests. Its design, calibration of the balance, and integration with the helicopter model has been performed at the Experimental Aerodynamics Department of the National Institute for Aerospace Technology (INTA). The balance is made of aluminum and contains strain gauges connected in seven Wheatstone bridges that provide an electrical output as a function of the deformation experienced, which can be measured and transformed into force values by appropriate calibration matrix obtained during the calibration process.

As shown in the 3D scheme of figure 4 and the real assembly in figure 5, HELIBAL was installed inside a PLA (Polylactic acid) 3D printed hollow fuselage of a Seaking SH-3 helicopter and a frame. The full assembly included also an Axi 2204 brushless motor that powers the helicopter rotor. Finally, a sting bar holds the helicopter assembly during wind tunnel tests. The balance helicopter axes for the measurement tests are also displayed in figure 4, with forces (F_X, F_y, F_z), that correspond to the aerodynamic drag force, side force and thrust generated by the helicopter rotor and torques (M_x, M_y, M_z) that represents the roll, pitch and yaw torques.

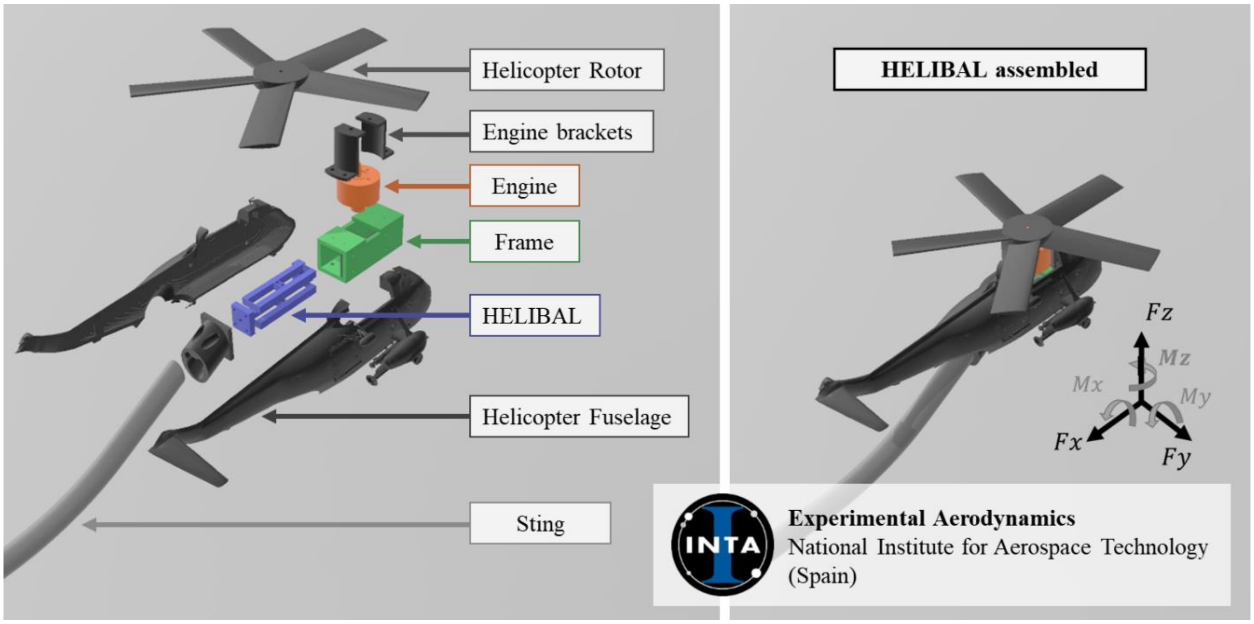

Fig. 4 Scheme of the internal balance inside the scaled helicopter model.

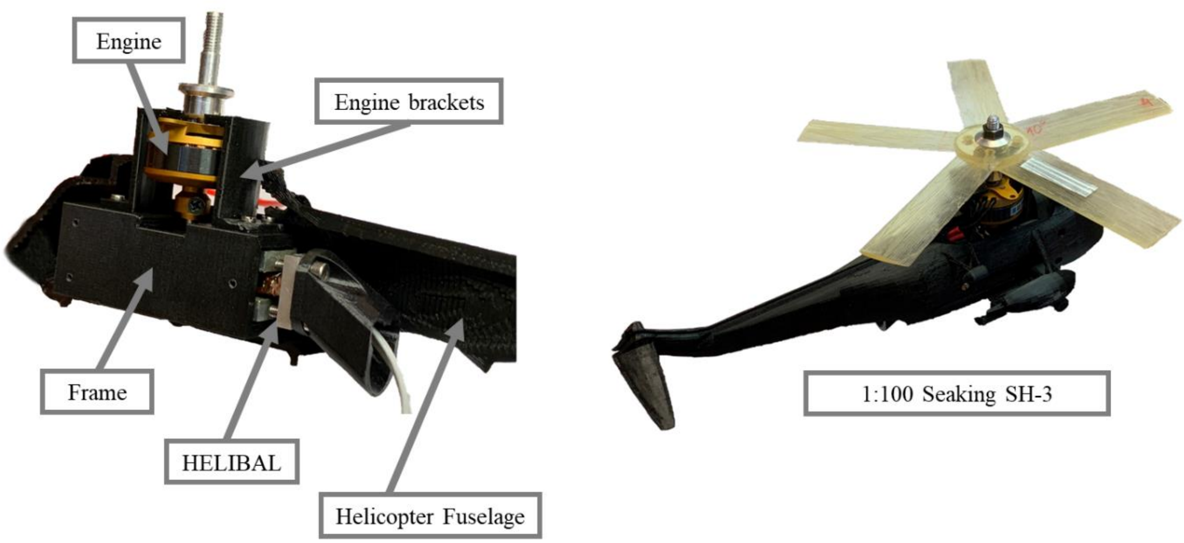

Fig. 5 Assembly of the internal balance inside the scaled helicopter model.

During wind tunnel tests, "MX Assistant V4" software is used to acquire the signals from the HELIBAL. The signals are recorded with a sampling rate of 100 Hz and processed with a 1Hz Butterworth IR low-pass filter to remove noise from the signals. At each position of the helicopter, the value of the signals is set to 0. Then, the wind tunnel and the helicopter rotor are turned on at the desired velocities, acquiring the signals given by the balance for 30 seconds. Each case recorded is a result of the average of the force and moment values calculated from the full report of the values.

3.4. Rotor flow similarity

To simulate the 1:100 scaled helicopter rotor, a 5 blades rigid rotor of 160 mm in diameter with symmetrical profiles is used. To ensure the flow similarity of the real helicopter and the scaled helicopter, the similarity of the thrust coefficient (C_T) and the advance ratio (J) must be achieved. The full-scale Sea King SH-3 helicopter has a thrust coefficient during hovering flight that can be obtained as,

$$C_T = \frac{T_{io}}{\rho(\Omega\mathrm{R})^2 S} = 6.47 \times 10^{-3} \tag{1}$$

where, the thrust is $T_{io} = W = (M \times g) = 69.9\ \mathrm{k}N$, the weight $M = 7130$ kg, air density $\rho = 1.225\ kg/m^3$, rotational speed $\Omega = 250$ rpm, radius $\mathrm{R} = 8$ m, rotor surface $S = 201\ \mathrm{m}^2$, and gravity $g = 9.81\ m/s^2$.

Table 1. Parameters used for helicopter flow similarity.

Parameter	Symbol	Full-Scale	Scaled model 1:100
Rotor radius	R	8 m	0.08 m
Angular Velocity	Ω	250 rpm	8,500 rpm
Rotor surface	S	201 m^2	0.0201 m^2
Thrust Coefficient	C_T	6.47×10^{-3}	6.47×10^{-3}
Advance Ratio	J	0.239	0.239

By performing several tests with the 1:100 scaled model varying the power (and therefore the rotor revolutions), a similar thrust coefficient of the scaled model $C_{Ts} = 6.47 \times 10^{-3}$ measured with the balance was obtained, when the power supply is 10 V and 2.5 A, resulting in $\Omega_s = 8{,}500$ rpm of the scaled rotor. Then, the momentum flow similarity is guaranteed.

It must be mentioned that although the flow similarity is guaranteed, the geometric similarity is not completely fulfilled, since the profile chord of the of the scaled rotor model is greater than the real one, with 20 mm chord, instead of the 4 mm that would correspond to 1:100 scale. This is necessary to have enough thrust to get the momentum quantity and to get the necessary stiffness when high revolutions are applied during tests.

Finally, the wind condition represented at the tests is the result of the sum of the navigation speed of the frigate (20 knots ~ 10 m/s) and intense wind velocity of 15 m/s, resulting in $U_\infty = 25$ m/s affecting the helicopter. To satisfy the similarity in the tunnel, a similarity of the advance ratio between the real helicopter (2) and the scaled model (3) must be also achieved,

$$J = \frac{2U_\infty}{\Omega \mathrm{R}} \tag{2}$$

$$J_s = \frac{2V_{tunel}}{\Omega_s \mathrm{R_s}} \tag{3}$$

where $\Omega = 250$ rpm, $\mathrm{R} = 8$ m, $\Omega_s = 8.500$ rpm, and $R_s = 0.08$ m. Then, $V_{tunel} = 8.50$ m/s is the velocity adjusted in the wind tunnel to satisfy the advance ratio similarity. A summary of the data used for similarity is shown in Table 1.

4. Results

4.1. PIV Velocity Contours

Particle Image Velocimetry (PIV) has been used for obtaining velocity contours of the flow around the helicopter in different positions of the three analyzed recovery maneuvers: stern (S), diagonal (D), and L-shaped (L), as shown in figure 6,

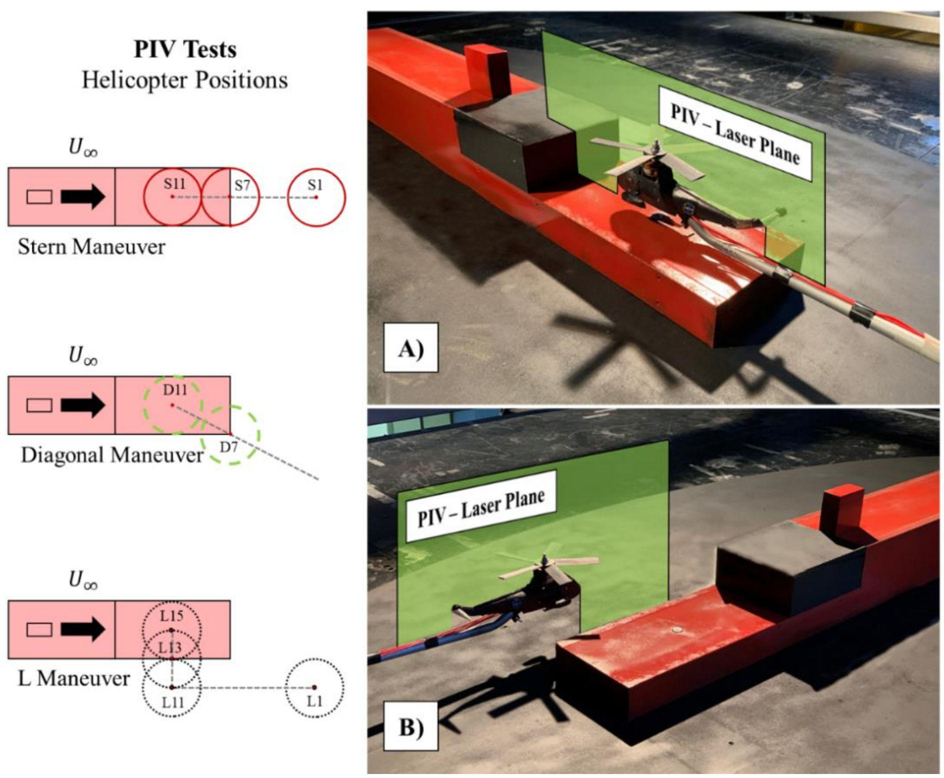

Fig. 6 Helicopter positions for PIV tests. A) PIV laser plane in S11. B) PIV laser plane in L11.

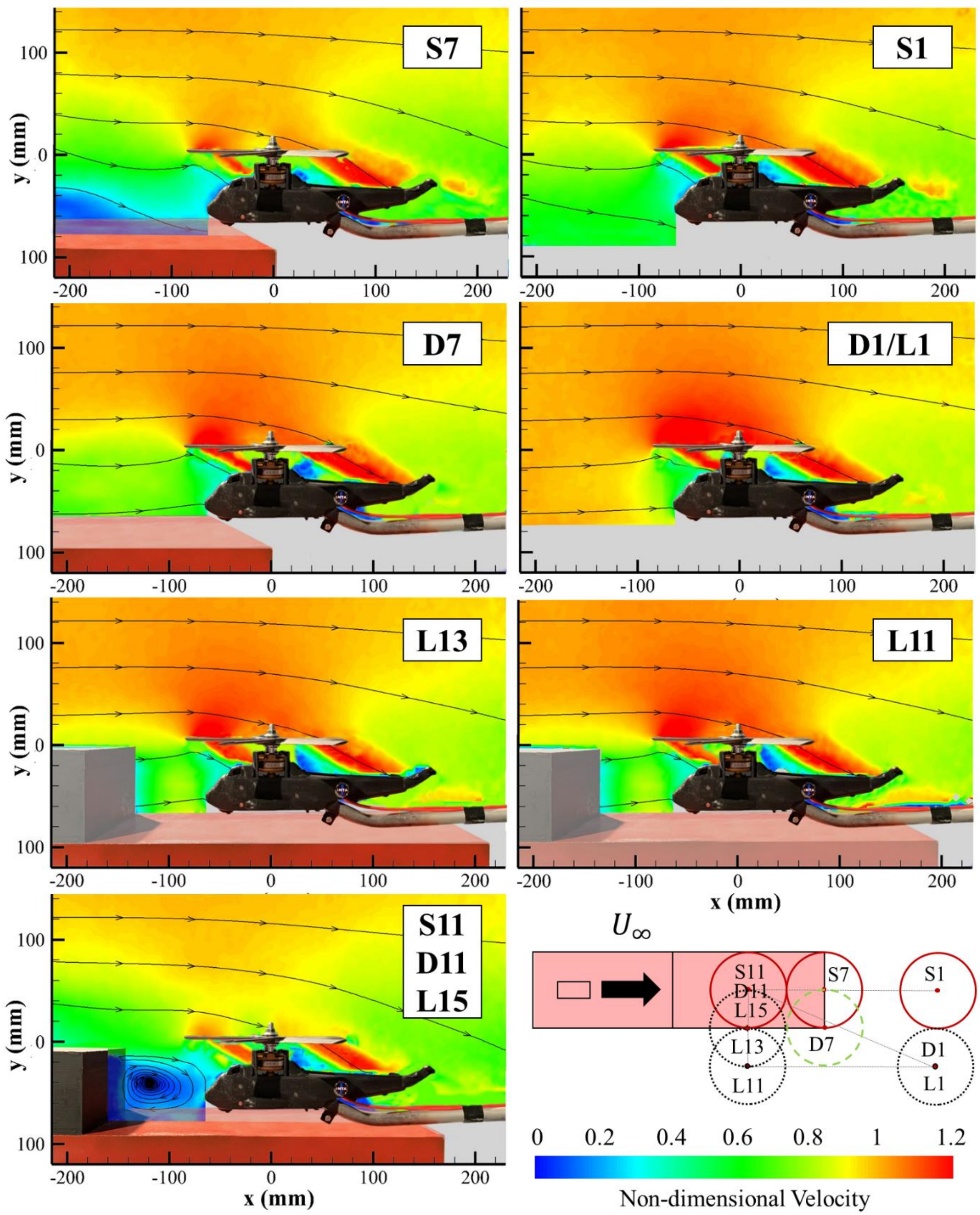

Fig. 7 PIV non-dimensional velocity contours for different helicopter positions.

The helicopter positions recorded are displayed schematically in Figure 6. The most representative positions have been chosen, i.e. outside of the frigate in the three maneuvers (S1, D1, L1), when the rotor is entering above the frigate flight deck (S7, D7, L11, and L13), and at the final position (S11, D11, L15). It is important to mention that the laser plane of the PIV is always aligned with the helicopter symmetry axis, as shown in Figure 6 A for the final point of the maneuvers (S11, D11, L15), and Figure 6 B for the L11 position. The averaged and non-dimensional velocity contours are also displayed in Figure 7.

During the stern maneuver the helicopter is affected by the wake generated from the frigate superstructure. The PIV contour of S1 shows incident velocities to the helicopter up to 50 % lower than the free-stream velocity. When the helicopter is positioned on the deck (S7), the velocities at the front of the helicopter are even lower, reaching non-dimensional values of 0.3. Unlike the previous case, the beginning of the diagonal and L-shaped maneuvers (D1 and L1) presents an incident flow similar to the free-stream, and is not affected by the presence of the frigate. Continuing with the diagonal maneuver at point D7, as the helicopter flies above the deck, it suffers a decrease in its incident velocities, but slightly less than in the case of the aft maneuver (S1 and S7).

Positions L11 and L13 shows a very similar flow condition with 0.4 to 0.8 incident non-dimensional velocities. The final position recorded (S11, D11, L15), that is the same for the three maneuvers, presents the flow detachment from the frigate hangar and the recirculation bubble generated in front of the helicopter. The incident flow to the helicopter has changed greatly compared to the other cases, which may negatively affect helicopter stability in this final phase of landing.

4.2. Force and torque measurements

In this section, 3,000 averaged values of forces and torque coefficients, obtained on each point of the maneuvers for the helicopter during the recovery procedure, are presented. A total of 37 helicopter positions have been analyzed: 11 for the stern maneuver (S1 to S11), 11 for diagonal maneuver (D1 to D11), and 15 for L-shaped maneuver (L1 to L15). A scheme of the helicopter and frigate positions analyzed is shown in figure 8. The distance from each point analyzed to the final point of the maneuvers (center of the flight deck) is also displayed. Considering that the maneuvers have been simulated for 7 different wind conditions (WOD = 0, ±10º, ±20º, ±30º), force and moment data have been obtained for a total of 259 cases.

The force and torque measurements can be expressed in terms of non-dimensional coefficients,

$$C_i = \frac{F_i}{\frac{1}{2}\rho(\Omega R)^2 S} \tag{4}$$

$$C_{mi} = \frac{M_x}{\frac{1}{2}\rho\Omega^2 R^3 S} \tag{5}$$

where $i = (x, y, z)$, F is the force in N, M is the torque in Nm, ρ is the air density, $\Omega = 8{,}500$ rpm, $R = 0.08$ m, $S = 0.0201$ m^2; C_x is the longitudinal force coefficient, C_y is the lateral force coefficient, C_z is the vertical force or thrust coefficient, C_{mx} is the roll coefficient, C_{my} is the pitch coefficient and C_{mz} is the yaw coefficient, according to the axes shown in figure 8.

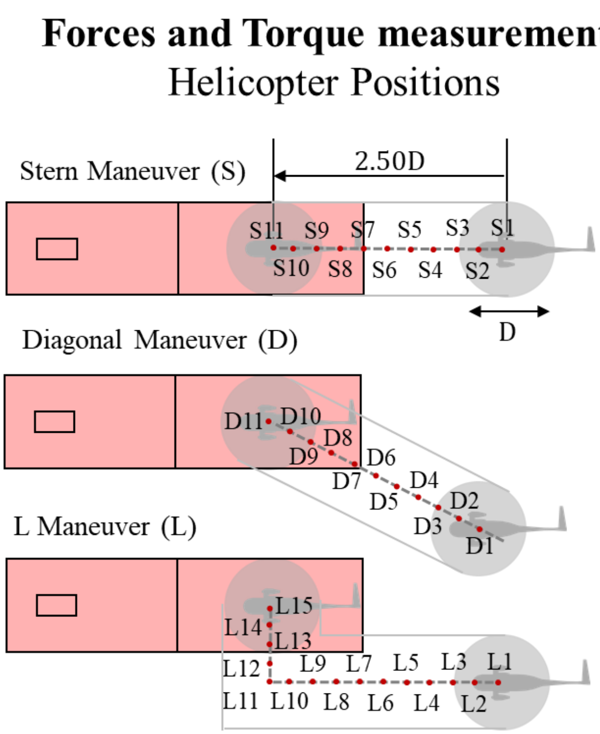

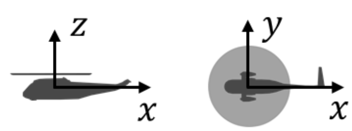

S	D	L	Distance to final
-	-	L1	3.50 D
-	-	L2	3.25 D
-	-	L3	3.00 D
-	-	L4	2.75 D
S1	D1	L5	2.50 D
S2	D2	L6	2.25 D
S3	D3	L7	2.00 D
S4	D4	L8	1.75 D
S5	D5	L9	1.50 D
S6	D6	L10	1.25 D
S7	D7	L11	1.00 D
S8	D8	L12	0.75 D
S9	D9	L13	0.50 D
S10	D10	L14	0.25 D
S11	D11	L15	0.00 D

Fig. 8 Forces and torques measurement points for stern, diagonal and L-shaped maneuver.

Results of forces and torques measured for WOD = 0º case are displayed in Figure 9, for positive wind angles are in figure 10, and for negative wind angles in figure 11. In all figures, the value measured on each point is represented with the averaged force or torque coefficient obtained in the corresponding position of the helicopter, measured as the distance to the final point of the maneuver in helicopter diameters (from 3.50 D to 0.00 D). As shown in the legend, points of each maneuver are represented using different marker (circles for stern - S, triangles for diagonal - D, and squares for L-shaped maneuver). Finally, force coefficients are displayed in different shades of green (C_x), orange (C_y), and blue (C_z). The torque coefficients are displayed with different shades of grey for C_{mx} and blue for C_{my}.

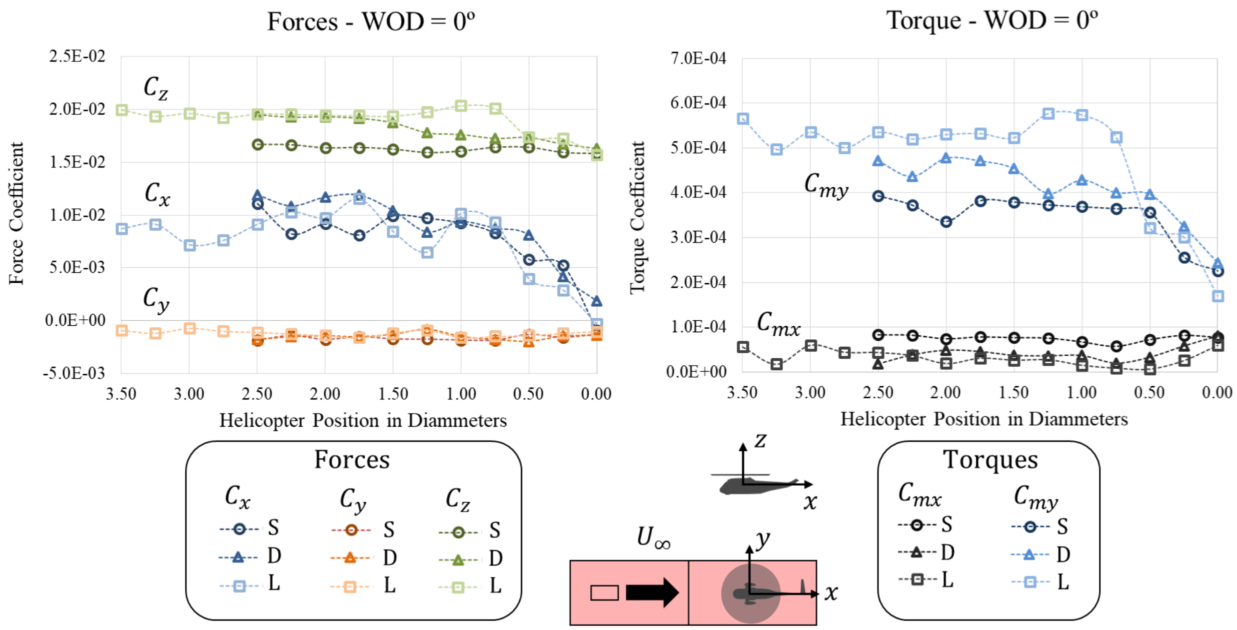

Fig. 9 Forces and torques measurement for stern, diagonal and L-shaped maneuver at WOD = 0º

In figure 9, the force coefficients for WOD = 0º, shows that the C_y values are practically zero during the maneuver, so the lateral force is not relevant for this wind condition. The longitudinal force coefficient C_x is subject to greater variation. In all three maneuvers the points remain around $C_x \sim 1.0E-2$, but a large drop occurs when the helicopter position is less than 1.00 rotor diameter, due to it is immersed in the wake of the frigate. Finally, the thrust coefficient C_z shows similar values for the beginning of D and L maneuvers ($C_z \sim 2.0E-2$). As the helicopter approaches the final point, the rotor thrust force is reduced to about 80 % of the initial value, with a coefficient $C_z \sim 1.6E-2$. The maneuver from stern (S) produces lower thrust values than the other two procedures, but with fairly constant values along the entire trajectory, due to being immersed in the wake of the frigate.

The same figure 9 shows the torque values for the roll (C_{mx}) and pitch (C_{my}) torques. There is hardly any roll torque during the three recovery maneuvers. However, the pitching torque has magnitudes up to 6 times higher, being positive and with a magnitude ordered from highest to lowest for the L, D and S maneuvers. As in the case of the forces, the presence of the frigate wake results in a large decrease in pitching moment at distances less than 1.00 diameter for the L maneuver, and less than 0.50 diameters for the D and S maneuver.

Next figure 10 displays the values of forces and torques obtained when the wind is from the port side of the frigate, i.e. positive WOD of 10º, 20º, and 30º. In general, the lateral force values C_y continue to be negligible for the 3 maneuvers tested. The longitudinal force coefficient C_x has higher values and variations, along the maneuvers. The thrust coefficient of the helicopter (C_z) is now very similar for all three maneuvers. However, C_z values are again a 5 to 10 % lower for the S than for the L and D maneuvers. Thrust and longitudinal force drop is also observed at the points of the final approach (0.50 to 0 position in diameters).

The roll torque C_{mx} is now important, since the wind now hits the helicopter by the left side. And obviously, its value is negative and greater in magnitude as the WOD increases. The pitching moment C_{my} is again always positive and quite similar in the three maneuvers. In addition, it is important to note that as it happens with the forces, there is a decrease in pitch values in the final approach (positions from 1.00 to 0 diameters). Specifically, the maximum variation in the final phase of the C_{my} is around 30 % for 10º, and up to 50 % for 20º and 30º.

Force and torque values when the wind comes from the starboard side (WOD = -10º, -20º, -30º) are displayed in figure 11. Again, lateral forces are low and with a C_y slightly negative due to the incidence of the wind on the right side of the helicopter during the procedures. The longitudinal coefficient C_x presents significant variations along the points of the maneuvers. In general, their values seem to be reduced with respect to WOD 0º and positive cases. This must be due to the fact that the wind now hits the frigate first, producing a wake that results in a reduction of the forces affecting the helicopter. The thrust coefficient C_z values are now much more uniform, and there are no large decreases in the final phase of the recoveries. However, the major difference compared to the previous cases is that now the greatest vertical force is generated during the S recovery (especially at -10º and -20º), with the D and L maneuvers with thrust values a 10 % lower during almost the entire trajectory. This change in the trend should be produced because maneuvers D and L are performed on the port side, and the incidence of the wind on the opposite side produces a decrease in the wind speeds incident to the rotor, which generates a decrease in thrust with respect to maneuver S (less affected by this phenomenon).

As the wind now hits the helicopter by the right side, there is a positive roll torque (C_{mx}) which, in general, takes higher values as the WOD angle increases. Pitch torque (C_{my}) is again positive, suffer important variations along the maneuvers, and again shows a decrease in its value as the final points of the maneuver are reached (from position 1.00 diameter to the final point).

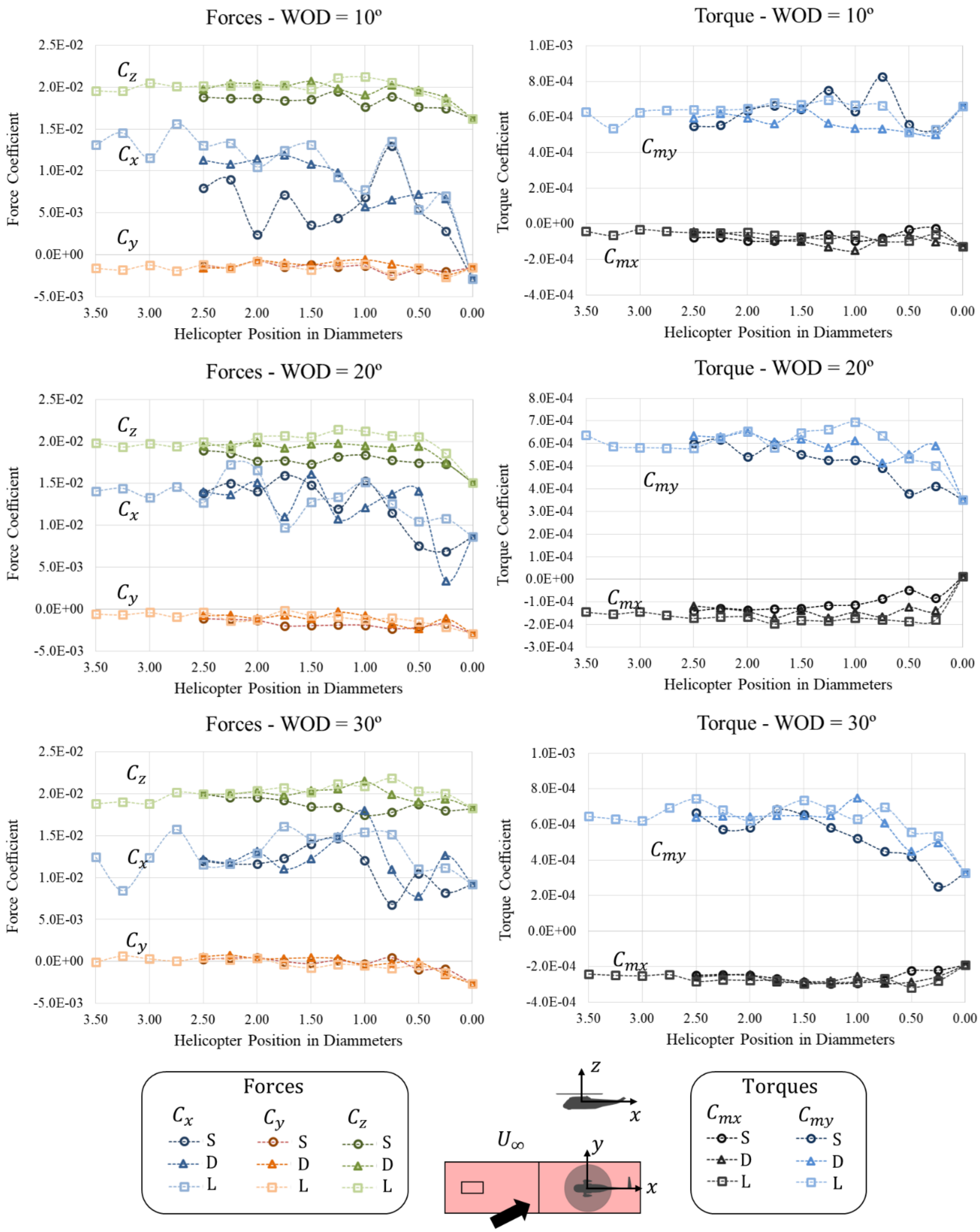

Fig. 10 Forces and torques measurement for stern, diagonal and L maneuver at WOD = 10º, 20º, and 30º.

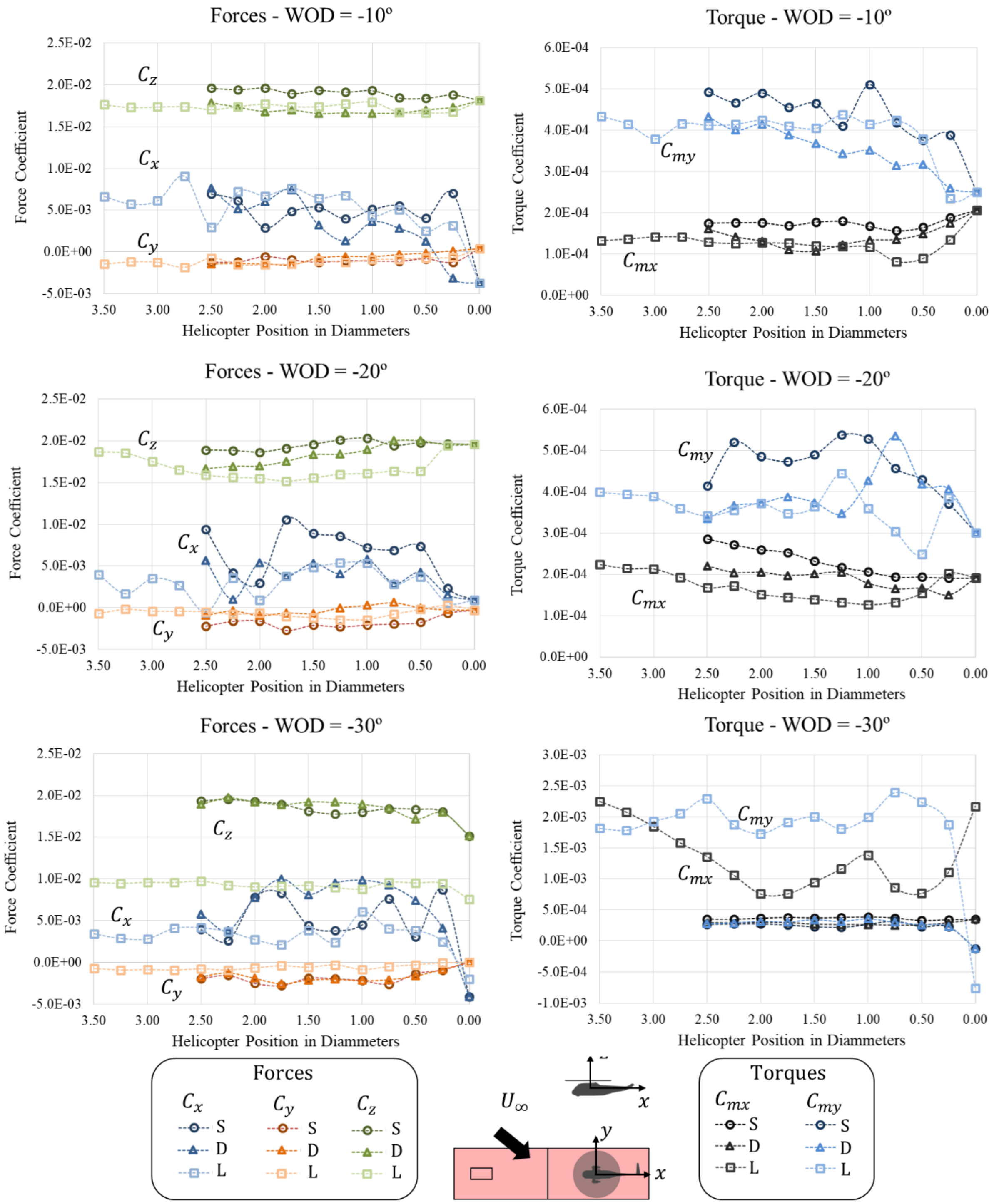

Fig. 11 Forces and torques measurement for stern, diagonal and L maneuver at WOD = -10º, -20º, -30º

In summary, it has been seen that the recovery maneuvers of the helicopter on a frigate causes changes in the helicopter flight condition. Especially, the longitudinal and thrust forces are the most affected by the wake of the ship.

In addition, the pitching moment is also greatly affected by positioning the helicopter behind the frigate superstructure. Finally, the roll moment is only important when the wind angle of incidence increases, either with positive or negative.

4.3. Pilot workload comparison

Once the magnitude of forces and moments have been analyzed, a comparison of the maneuvers is going to be made in this section. For this purpose, as there is a time record at each of the points of the recovery maneuvers, the standard deviation (σ) of the forces can be quantified. This standard deviation can be related to the pilot's workload, since the greater the variations, the greater would be the corrections made by the pilot to control the helicopter at each point.

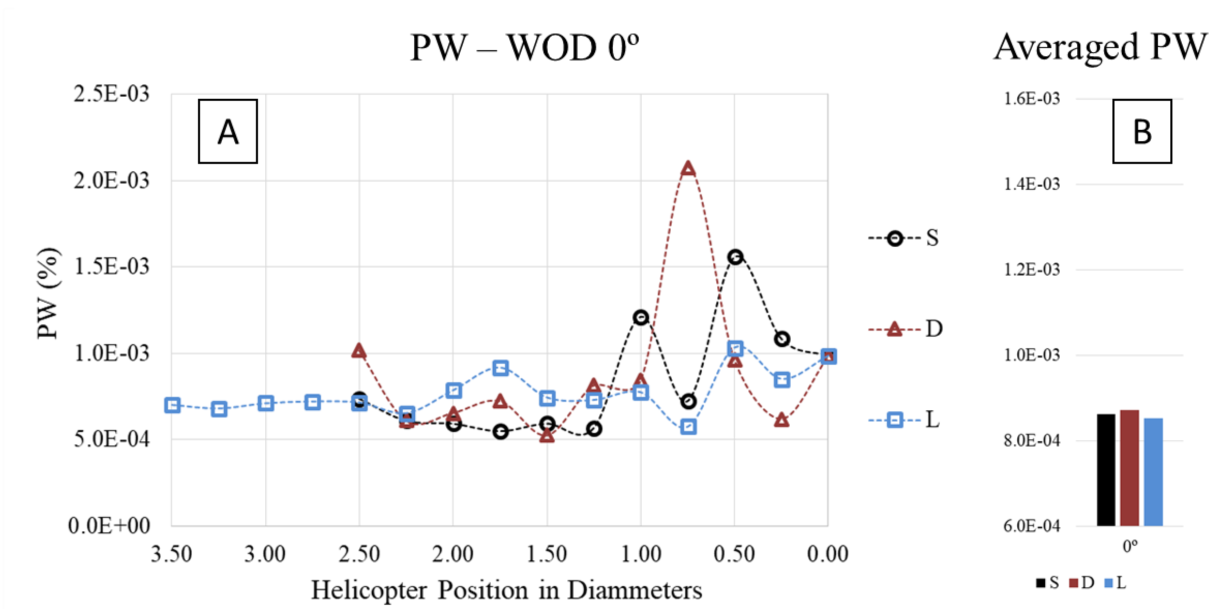

Fig. 12 A) PW parameter calculated for each point of S, D and L maneuvers at WOD = 0º B) Averaged PW for S, D, and L maneuvers.

The helicopter pilot workload (PW) can be analyzed on each point of the maneuvers through standard deviations [39] of force components with the following parameter,

$$PW = \sigma_{Cx} + \sigma_{Cy} + \sigma_{Cz} \quad (6)$$

where σ_{C_x}, σ_{C_y}, σ_{C_z} are the standard deviations of the longitudinal, lateral, and thrust coefficients.

As an example, figure 12 A shows the value of PW calculated on each point of the three maneuvers at wind conditions WOD = 0º. At the beginning of the maneuvers, and when the rotor continues hovering outside of the frigate

(3.50 to 1.00 diameters), PW values are low. After that, peaks appear for all three maneuvers. A very intense peak for 0.75D is presented in D maneuver, several intense peaks for S procedure (1.00, 0.50, and 0.25D), and more moderate peaks for the L maneuver. Finally, PW can be averaged with all the points in each maneuver, from 2.50 D to 0.00 D (Figure 12 B). From this average it is possible to conclude that in WOD = 0º case, the pilot workload (PW) derived from the deviations obtained in the forces with the balance is lower for the L maneuver, followed by the S and D maneuvers, respectively. The same calculation has been performed for all angles tested, and the results are shown in figure 13.

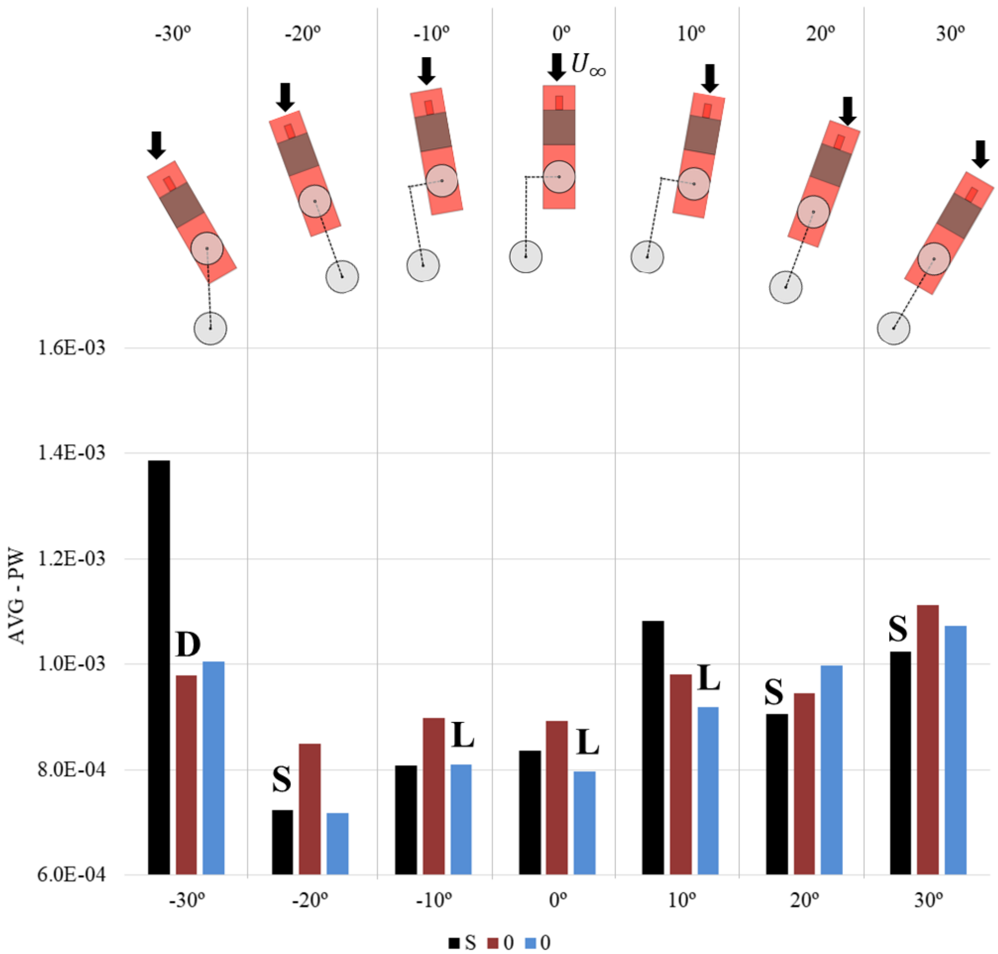

Fig. 13 Comparison of averaged PW for S, D, and L recovery maneuvers and all WOD angles tested.

Thus, it is possible to conclude that, from the point of view of deviations, if the helicopter recovery operation is performed with WOD = 0º, or low wind angle conditions ($\pm 10^o$), the L maneuver produces the lower pilot workload (PW). This result is logical, as during the L-shaped maneuver the helicopter performs most of the maneuver on the downwind side, and without being immersed in the wake of the frigate. Increasing more the WOD angle, and when the wind is positive (port side), the most optimal maneuver is S with lower values of force deviations. Finally, if the wind over deck is moderately negative (wind from starboard side), best results are obtained for S maneuver at -20º, and for D or L maneuver for -30º. Again, the results seems logical, given that by stern (S) or diagonal (D) maneuvers, the helicopter avoids being in the frigate's wake during negative WOD conditions.

5. Conclusions

The goal of this paper was to present wind tunnel measurements of the helicopter and frigate aerodynamic interaction, during three paths of recovery maneuvers: stern, diagonal and L-shaped. A 1/100 scaled models of frigate and a motorized helicopter is tested extracting PIV images of the flow and using an internal six-component balance for force measurements. Seven wind conditions have been tested, simulating wind over deck (WOD) conditions between 0 and 30º, from the port and starboard side.

PIV results have shown that at the beginning of the stern maneuver the helicopter is slightly affected by the wake generated from the frigate superstructure, and highly affected when the helicopter is positioned above the deck. On the contrary, the beginning of the diagonal (D) and L-shaped maneuvers are not affected by the presence of the frigate. It is important to mention that final positions for the three maneuvers are immersed in the flow detachment from the frigate hangar and the recirculation bubble generated.

From the forces and moments measurements, it has been seen that the recovery maneuvers of the helicopter on a frigate causes changes in the helicopter flight condition. Longitudinal and thrust coefficients are the most affected by the wake of the ship. In addition, the pitching moment is also affected when the helicopter is behind the frigate superstructure. Finally, the roll moment is also important when the wind angle of incidence increases, either with positive or negative WOD angles.

Specifically, from the cases of WOD = 0º,

- There is a drop in longitudinal forces near the final point, and the rotor thrust is reduced to about 80 %
- The maneuver from stern (S) produces lower thrust values than the other two, due to being immersed in the wake of the frigate.
- There is no roll torque and the pitch torque is positive and with a magnitude ordered from highest to lowest for the L, D and S maneuvers.

For positive WOD angles,

- Longitudinal force coefficient has high variations along the maneuvers
- Thrust coefficient of the helicopter is again a 5 to 10 % lower for the S than for the L and D final part of the maneuvers.
- Roll torque is negative, since the wind hits the helicopter by the left side, and increases in magnitude as the WOD is higher. Pitching moment is positive and quite similar in the three maneuvers.

For negative WOD angles,

- Lateral forces are low and negative due to the incidence of the wind on the right side of the helicopter
- Longitudinal forces shows significant variations and reduced (due to the helicopter is inside the frigate wake) with respect to 0º and positive WOD cases.
- Thrust coefficient is more uniform, and there are no large decreases in the final phase of the recoveries..
- Positive roll torque with higher values as the WOD angle increases. Pitch torque is again positive, suffer important variations along the maneuvers, and decrease its value at the final points.

At the end, a pilot workload (PW) estimation has been made by using a parameter, based the standard deviations of the forces measured. At the beginning of the maneuvers, and when the rotor continues hovering outside of the frigate, PW values are low. After that, peaks of PW appear for the three maneuvers. From the averaged results of pilot workload, at low wind over deck angles, L maneuver is the best. If the helicopter recovery operation is done with strongly positive wind angles (port side), the most optimal maneuver is S, with lower values of force deviations. Finally, when the wind angle is negative (starboard side), the results have shown that S maneuver is adequate for -20º, and D o L maneuvers for -30º. The results presented in this paper could be used to improve the safety of operations by choosing one approach procedure or another, depending on the sailing and incident wind conditions.

Acknowledgments

The authors would like to thank the staff of the Experimental Aerodynamics department of INTA who participated in the tests presented in this paper. This study is included in the “Termofluidodinámica” program 464A 64 1999 14 205 0005 of the Spanish Ministry of Defense with INTA internal code IDATEC S.IGB21001.

References

[1] Łusiak, Tomasz & Dziubinski, Adam & Szumański, Kazimierz. (2009). Interference between helicopter and its surroundings, experimental and numerical analysis. Task Quarterly. 13.

[2] Rowe S J et al 2001 The response of helicopters to aerodynamic disturbances around offshore helidecks RAeS Conf. on Helicopter Operations in the Maritime Environment (London, UK).

[3] Kääriä, C., Y. Wang, M. White and I. Owen. 2013. An experimental technique for evaluating the aerodynamic impact of ship superstructures on helicopter operations. Ocean Engineering. 61:97-108.

[4] Bardera-Mora, R., León Calero, M., and García-Magariño, A., "Aerodynamic effect of the aircraft carrier island on flight deck flow with Cross Wind," Proceedings of the Institution of Mechanical Engineers, Part M: Journal of Engineering for the Maritime Environment, vol. 232, 2017, pp. 145–154. 10.1177/1475090216689172

[5] Healey, J. V. 1992. Establishing a database for flight in the wakes of structures. Journal of Aircraft. 29(4):559-564. Journal of the American Helicopter Society

[6] Dooley, G. M., Krebill, A. F., Martin, J. E., Buchholz, J. H. J., and Carrica, P. M., "Structure of a Ship Airwake at Multiple Scales," AIAA Journal, Vol. 58, No. 5, 2020, pp. 2005–2013. https://doi.org/10.2514/1.J058994

[7] Thedin, R., Murman, S., Horn, J., and Schmitz, S., "Effects of Atmospheric Turbulence Unsteadiness on Ship Airwakes and Helicopter Dynamics," Journal of Aircraft, Vol. 57, No. 3, 2020, pp. 534–546. https://doi.org/10.2514/1.C035643

[8] Yuan, W., Wall, A., & Lee, R. (2018). "Combined numerical and experimental simulations of unsteady ship airwakes". Computers & Fluids, 172, 29-53.

[9] Crozon, C., Steijl, R., and Barakos, G. N., "Numerical Study of Helicopter Rotors in a Ship Airwake," Journal of Aircraft, Vol. 51, No. 6, 2014, pp. 1813–1832. https://doi.org/10.2514/1.C032535

[10] Brownell, C., L. Luznik, M. Snyder, H. Kang and C. Wilkinson. 2012. "In Situ Velocity Measurements in the Near-Wake of a Ship Superstructure". Journal of Aircraft. 49(5):1440-1450.

[11] Bardera, R., "Flow field velocity on the flight deck of a frigate," Proceedings of the Institution of Mechanical Engineers, Part G: Journal of Aerospace Engineering, vol. 228, 2014, pp. 2674–2680.

[12] Bardera-Mora, R., Barcala-Montejano, M., Rodríguez-Sevillano, A., de Diego, G., & de Sotto, M. (2015). "A spectral analysis of laser Doppler anemometry turbulent flow measurements in a ship air wake". Proceedings Of The Institution Of Mechanical Engineers, Part G: Journal Of Aerospace Engineering, 229(12), 2309-2320.

[13] Lee, R. and S. Zan. 2005. Wind Tunnel Testing of a Helicopter Fuselage and Rotor in a Ship Airwake. Journal of the American Helicopter Society. 50(4):326-337.

[14] Lee, R. and S. Zan. 2004. Unsteady aerodynamic loading on a helicopter fuselage and rotor in a ship airwake. American Helicopter Society. 49(2):149-159.

[15] Van Muijden, J., Boelens, O., van der Vorst, J., and Gooden, J., "Computational Ship Airwake Determination to Support Helicopter-Ship Dynamic Interface Assessment," 21st AIAA Computational Fluid Dynamics Conference, AIAA Paper 2013-3078, 2013. https://doi.org/10.2514/6.2013-3078

[16] Wakefield, N. H., Newman, S. J., and Wilson, P. A., "Helicopter Flight Around a Ship's Superstructure," Proceedings of the Institution of Mechanical Engineers, Part G: Journal of Aerospace Engineering, Vol. 216, No. 1, 2002, pp. 13–28. https://doi.org/10.1243/0954410021533391

[17] Wadcock, A. J., G. K. Yamauchi, J. T. Heineck, M. J. Silva and K. R. Long. 2004. "PIV Measurements of the Wake of a Tandem-Rotor Helicopter in Proximity to a Ship". National Aeronautics and space administration moffett field CA AMES research center.

[18] Doane, S. R. and D.A. Landman. 2012. "A wind tunnel investigation of ship airwake/rotor downwash coupling using design of experiments methologies". In: Proceedings of the 50th AIAA Aerospace Sciences Meeting including the New Horizons Forum and Aerospace Exposition. 2012-0767.

[19] Silva M J et al 2004 Wind tunnel investigation of the aerodynamic interactions between helicopter and tilt-rotors in a shipboard environment. American Helicopter Society 4th Decennial Specialist's Conf. on Aeromechanics (San Francisco, CA).

[20] Derby M R and Yamauchi G K 2003 Design of 1/48th-scale models for ship-rotorcraft integration studies 21st AIAA Applied Aerodynamics Conf. (Orlando, FL) AIAA-2003-3952.

[21] Wang Y, Curran J, Padfield G D, Owen I. AirDyn: an instrumented model-scale helicopter for measuring unsteady aerodynamic loading in airwakes. Measurement Science and Technology. IOP Publishing. DOI: 10.1088/0957-0233/22/4/045901

[22] Kaaria C H, Forrest J S, Owen I. The virtual AirDyn: a simulation technique for evaluating the aerodynamic impact of ship superestructures on helicopter operations. Aeronautical Journal. 117 (1198). Pp 1233-1248. 2013

[23] Taymourtash, N., Zanotti, A. Gilbertini, G. Quaranta, G. Simulation and Testing of Helicopter-ship Aerodynamic Interaction. 47th European Rotorcraft Forum, Glasgow, Scotland, 7-9 September, 2021.

[24] Thedin, R., Kinzel, M. P., Horn, J. F., and Schmitz, S., "Coupled Simulations of Atmospheric Turbulence-Modified Ship Airwakes and Helicopter Flight Dynamics," Journal of Aircraft, Vol. 56, No. 2, 2019, pp. 812–824. https://doi.org/10.2514/1.C035158

[25] Memon,W. A., Owen, I., and White, M. D., "Motion Fidelity Requirements for Helicopter-Ship Operations in Maritime Rotorcraft Flight Simulators," Journal of Aircraft, Vol. 56, No. 6, 2019, pp. 2189–2209. https://doi.org/10.2514/1.C035521

[26] Watson, N. A., Owen, I., and White, M. D., "Piloted Flight Simulation of Helicopter Recovery to the Queen Elizabeth Class Aircraft Carrier," Journal of Aircraft, Vol. 57, No. 4, 2020, pp. 742–760. https://doi.org/10.2514/1.C035733

[27] Forrest, J., Kaaria, C., and Owen, I., "Evaluating Ship Superstructure Aerodynamics for Maritime Helicopter Operations Through CFD and Flight Simulation," Aeronautical Journal, Vol. 120, No. 1232, 2016, pp. 1578–1603. https://doi.org/10.1017/aer.2016.76

[28] Forsythe, J., Lynch, E., Polsky, S., and Spalart, P., "Coupled Flight Simulator and CFD Calculations of Ship Airwake Using Kestrel," 53rd AIAA Aerospace Sciences Meeting, AIAA Paper 2015-0556, 2015. https://doi.org/10.2514/6.2015-0556

[29] Foeken, M. Pavel, M. D. Investigation on the simulation of helicopter/ship operations. Faculty of Aerospace Engineering, Delft University of Technology Kluyverweg 1, 2629 HS, Delft, The Netherlands.

[30] Raffel, M. C. Willert, F. Scarano, C. Kähler, S. Wereley and J. Kompenhans. 2007. Particle Image Velocimetry. Springer.

[31] Adrian, R. and J. Westerweel. 2011. Particle Image Velocimetry. Cambridge: Cambridge University Press.

[32] Prasad, A. K. 2000. Particle image velocimetry. CURRENT SCIENCE-BANGALORE-, 79(1), 51-60.

[33] Adrian, R. J. 1991. Particle-imaging techniques for experimental fluid mechanics. Annual review of fluid mechanics, 23(1), 261-304.

[34] Adrian, R. J., & Westerweel, J. 2011. Particle image velocimetry (No. 30). Cambridge University Press.

[35] S. J. Zan. 2000. Surface Flow Topology for a Simple Frigate Shape. Canadian Aeronautics and Space Journal. 47:33-43

[36] Bardera, R. 2014. Experimental Investigation of the Flow on a Simple Frigate Shape (SFS). The Scientific World Journal, 2014:1-8.

[37] Yuan W., R. Lee and A. Wall 2016. Simulation of Unsteady Ship Airwakes Using Openfoam. In : 30th Congress of the International Council of the Aeronautical Sciences. DCC, Daejeon, Korea: September 25-30.

[38] Yuan, W., A. Wall and R. Lee. 2018. Combined numerical and experimental simulations of unsteady ship airwakes. Computers & Fluids, 172: 29-53.

[39] Garner, W. Murphy, M. 1976 "Pilot Workload and fatigue: a critical survey of concepts and assessment techniques" Nasa Technical Note D-8365.